energies

MDPI

Article

Energy and Exergy Analyses of a Novel Combined Heat and Power System Operated by a Recuperative Organic Rankine Cycle Integrated with a Water Heating System

Babras Khan [1] and Man-Hoe Kim [2,*]

[1] School of Mechanical Engineering, Pusan National University, Pusan 46241, Korea
[2] School of Mechanical Engineering & IEDT, Kyungpook National University, Daegu 41566, Korea
* Correspondence: manhoe.kim@knu.ac.kr; Tel./Fax: +82-53-950-5576

Abstract: This study reports the thermodynamic analysis of a high-temperature recuperative organic Rankine cycle comprising a water heating system that can provide a net power of 585.7 kW and hot water for domestic use at 35 °C. The performance was analysed using seasonal ambient temperature and water temperature data from Seoul, South Korea. The working fluid was separated into two different mass fractions after emerging from the turbine 1 outlet; one fraction provided heat to recuperate the organic Rankine cycle, and the other fraction was transferred to the water heating system for heating water. Mass fractions were balanced based on the projected seasonal need for hot water. Four working fluids with high critical temperatures and five working fluids with low critical temperatures were examined for top and bottom cycles, respectively. Chlorobenzene was selected for the top cycle and R601 was selected for the bottom cycle. The system achievement in individual months was analysed using thermal efficiency and exergy efficiency. Moreover, the performances of the hottest (low hot water demand) and coldest (high hot water demand) months were analysed.

Keywords: exergy efficiency; exergy destruction; water heating system; recuperative ORC; mass fraction

Citation: Khan, B.; Kim, M.-H. Energy and Exergy Analyses of a Novel Combined Heat and Power System Operated by a Recuperative Organic Rankine Cycle Integrated with a Water Heating System. *Energies* **2022**, *15*, 6658. https://doi.org/10.3390/en15186658

Academic Editor: Andrea Frazzica

Received: 3 August 2022
Accepted: 9 September 2022
Published: 12 September 2022

1. Introduction

The global energy demand continues to increase with the depletion of fossil fuel resources and the risks of climate change. Greenhouse gases produced by the burning of fossil fuels pose major risks to the environment and are a serious unforeseeable cause of global climate change. Addressing this global energy and environmental challenges requires improving energy efficiency in the industry [1,2]. All energy-related issues, including resources, demand, supply and applications, were of global concern. Implementing heat efficient practices and utilizing industrial waste heat and renewable energy sources are possible practice to improve industrial energy efficiency [3]. Advances in technology have made renewable energy and low-grade waste heat sources a prime candidate for a variety of applications such as power generation, cooling and heating. Energy technology perspective analysis offers a comprehensive, long-term view of energy system trends and technologies essential to meet goals for affordable, secure, and low-carbon energy. Therefore, there is an urgent need for alternative energy sources to address this insurmountable global problem. Researchers have focused on diverse and effective alternative renewable energy resources for energy production; heat sources can be diverse, including solar energy, energy from human excreta, biogas combustion, and waste heat from industrial processes [4].

South Korea's energy sector is dominated by fossil fuels. In 2018, the total fossil fuel supply was 85%, of which energy imports accounted for 84% of total fuel supply and industrial energy accounted for 55% of total energy consumption. The South Korean government pledged to promote South Korea's energy transition by increasing the proportion of renewable electricity to 20% by 2030 and 30–35% by 2040 [5]. The government plans to reduce the number of nuclear and coal-fired power plants to achieve clean and

safe energy and improve air pollution [6]. The organic Rankine cycle (ORC) has been a favourable approach for using renewable energy because of its thermodynamic properties. It can acquire heat from low-grade energy sources and reduce fossil fuel depletion and greenhouse gas emissions [7].

In the past two decades, ORC technology has been a topic of extensive research. An ORC system is integrated with combined heat and power (CHP) system by introducing a cold sink to improve the efficiency of the entire system [8]. CHP systems, in terms of energy savings and environmental protection, are the prime substitutes for traditional energy production systems. Furthermore, these systems can achieve many dynamic, environmental, and social goals: reducing greenhouse gas emissions, promoting decentralisation of energy production and energy security, and reducing investment in transmission and distribution networks to decrease energy costs for consumers [9]. Low and medium levels of waste or renewable heat can be converted into useful power or recycled for direct heating of buildings (for hot water or space heating), or a combination of both. Many technologies have been developed for converting low-energy heat into electrical energy [10].

CHP systems have gained more attention than standard power plants because they can achieve maximum productivity. ORC-based CHP systems are suitable for domestic heating activities. Acha et al. [11] reported an ideal design and functioning of transmitted energy mechanisms in buildings. A combination of cogeneration and distributed energy systems, such as ORC or absorption cooler (ARC), was technically selected for operation (an optimisation model). White et al. [12] correlated cost and component size and generated a framework based on computer-aided CAD–ORC. Freeman et al. [13] optimised a solar-based CHP system with a maximum power output that was higher than the earlier reported largest consecutive mean power (122 W). Chatzopoulou and Markides [14] presented a thermodynamic optimisation analysis of an IC engine based on an ORC–CHP system for obtaining maximum power with minimum fuel consumption. Oyewunni et al. [15] recovered waste heat from flue gas over a temperature range of 150 °C to 330 °C and mass flow rates of 120 kg/s and 560 kg/s using an optimised ORC–CHP configuration. Axial power was generated by the thermodynamic conversion of the ORC turbine, and the generated heat was used for residential or industrial heating by the cooling flow of the ORC condenser. Aziz et al. [16] designed a system in which a fraction of hot steam from a high-temperature ORC was discharged from the turbine for heating water to 35 °C, while the other part of the steam operated another ORC system.

Considering the limited cooling capacity, ORC systems have higher efficiency [17] indicating that less cooling is required for generating the same power. Researchers have stressed recuperative ORC systems because they are more efficient than basic ORC systems. Zhao et al. [18] studied a basic ORC model and three recuperative ORC models with different heat transfer rates in combination with an engine model. The steady-state results showed that an increase in the recuperative rate decreased the cooling heat while the net output power increased. The use of recuperators has become important for ORCs that use working fluids with high molecular complexity [19]. A recuperative solar Rankine cycle using R245fa, a dry working fluid, was presented by Wang et al. [20] and demonstrated favourable solubility, durability, stability, and safety characteristics.

There are numerous working fluids for ORC engines for a variety of applications. Choosing the appropriate working fluid has a significant impact on the efficiency, design, and sizing of individual components, as well as the economics of the plant. Jang and Lee [21] studied a biomass-based ORC–CHP system on a domestic scale to evaluate the optimal operating conditions with eight working fluids. They initially screened 107 fluids considering their environmental and thermodynamic properties. Four micro ORC–CHP configurations were used to analyse the system performance and obtain an optimised prime function. Working fluids in Group A (HCFC-141b, cyclopentane, isopentane, n-pentane, and diethyl ether) exhibited the lowest refrigerant mass flow rate, highest ORC efficiency, lowest heat input to the evaporator, and highest CHP efficiency. Yagli et al. [22] used R245fa in supercritical and subcritical ORCs to obtain waste heat from CHP engines with biogas

as fuel. The performance of the supercritical ORC was better than that of the subcritical ORC with a network output power of 81.52 kW, thermal efficiency of 15.93%, and exergy efficiency of 27.76%.

ORC-based CHP systems with a working fluid heated by a source derived from the heat rejected by a condenser expanded in a turbine to generate electricity have also been reported. Moreover, ORCs have been used as a bottom cycle to utilise the exhaust gas from gas turbines or engines. Additionally, high-temperature and high-pressure steam leaving the ORC turbine is especially used for regeneration purposes. Work in this field emphasises a novel ORC-based CHP system in which a fraction of hot steam is discharged from the high-temperature ORC turbine This steam is utilised to heat water up to 35 °C. Conversely, recuperative ORC with a relatively low-temperature fluid is operated using the other fraction of hot steam. Thus, the system selected Seoul (South Korea) as a reference location and collected water temperature and ambient air data to study the total thermal power needed to supply hot water to houses. Monthly changes in temperature result in changes in the monthly demand for hot water; consequently, the system generates a portion of electricity and thermal power in the respective month of the year. In this context, comprehensive thermal performance analysis of the system is presented.

2. Materials and Methods

The schematic layout of a power generation system appended with a water heating system (WHS) is shown in Figure 1. The power generation system comprises a dual ORC system: the top cycle is a simple ORC (SORC), and the bottom cycle is a recuperated ORC (RORC), which is attached to an adjustable water heating system. The SORC and RORC use working fluids with high critical temperature and low critical temperature, respectively. The entire system supplies electric power and hot water to Seoul. The basic motive of the proposed system is to examine the result of the specific performance, such as power output, heating capacity, energy, and exergy efficiencies of the power system, with a change in water temperature and ambient temperature for the entire year.

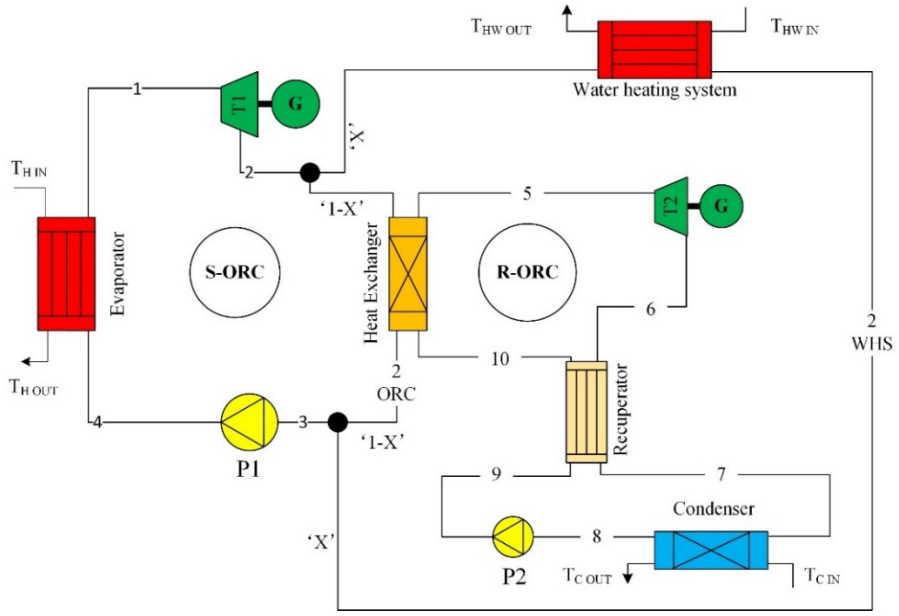

Figure 1. Schematic of dual ORC integrated with WHS.

The mass fraction x value of fluid 1 at the turbine outlet allows more fluid from the SORC to be used for heating water during winter as the hot water demand increases during this season. Contrarily, the mass fraction x value is retuned to generate more work by the RORC in summer than in winter. This is because less water has to be heated during summer. The mass fraction x value of fluid 1 was calculated using Equation (6)

for the respective months. After the precise recording of the monthly water temperature and ambient temperature data [23] of Seoul, the monthly mass flow rate was determined. Table 1 lists the monthly ambient temperature data and the essential flow rate for hot water, as well as the ratio of mass fraction x of fluid 1 used for heating water in the WHS. The values shown in the table vary depending on the requirement of hot water.

Table 1. Monthly input parameters for Seoul, South Korea.

Months	Ambient Temperature (°C)			$T_{water\ (month)}$ (°C)	m_{HW} (kg/s)	'x' (%)
	Max	Min	Avg			
January	1.0	−7.7	−3.5	6.6	9.5	75.52
February	4.1	−5	−0.8	4.4	9.0	75.18
March	9.8	−0.5	4.2	3.8	6.5	53.42
April	16.3	5.6	10.7	6.1	6.0	42.84
May	22	11.6	16.5	10.5	5.8	35.16
June	26.3	17.3	21.5	15	5.5	25.93
July	27.7	21.4	24.2	20	5.0	18.19
August	28.4	21.7	24.8	23.3	4.8	14.22
September	24.6	16.3	20.3	24.4	6.5	21.02
October	18.5	9	13.6	21.1	7.0	28.29
November	10.4	1.6	5.8	16.6	7.5	42.44
December	2.8	−5.4	−1.5	11.6	10.0	70.06

2.1. Cycle Process

The dual ORC integrated with a WHS (ORC–WHS) comprises two turbines, two pumps, five heat exchangers, and one mixer as shown in Figure 1. Pump 1 raises fluid 1 to the desired pressure in the evaporator where heat is transmitted from transfer oil to fluid 1. Fluid 1 passes across turbine 1. Apart from expansion, the mass fraction x of fluid 1 flows to the water heating system, and the remaining portion proceeds to the heat exchanger. Water is heated to 35 °C by mass fraction x that flows across the WHS and returns to the mixer. In the mixer, mass fraction x is mixed with the other part of the heat transfer fluid from the heat exchanger to regenerate fluid 1. Fluid 1 is returned to pump 1 to complete and continue the cycle. The heat exchanger transfers heat to fluid 2 for operating the RORC by expansion in turbine 2. Exhaust heat is released to the recuperator, which acts as an energy saving function. This extracts the exhaust heat to preheat the fluid entering the combustion system. Thus, the heating load on the system is reduced. The cycle is finally completed by passing the fluid through the condenser to dissipate heat and increase the pressure through pump 2.

2.2. Energy Analysis

Figure 2 presents the temperature–entropy (T–S) diagram, which elucidates the thermodynamic process of the cascading ORC–WHS. The analysis was simplified assuming the following conditions.

- Pressure drops in the evaporator, heat exchanger, condenser, and connecting pipes were ignored.
- All flow devices of the system were assumed to be at a steady state.
- Working fluids entered each pump as a saturated liquid.
- No stray heat was transferred within components.
- No heat was lost in the mixer.

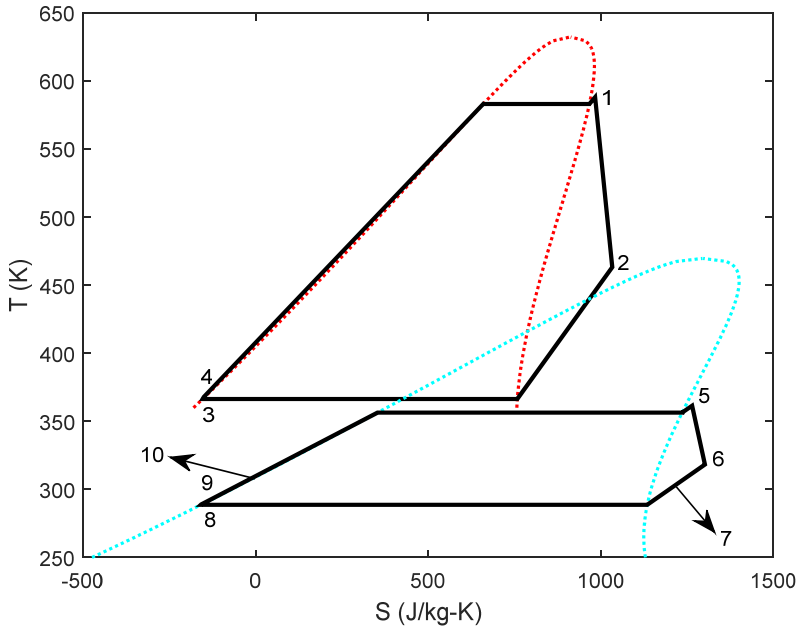

Figure 2. Temperature-entropy diagram of cascading ORC-WHS.

The above assumptions were intended to avoid intricate analysis. The purpose of this article is to propose a brief and fundamental analysis of a combined heat and power system under various temperatures and conditions throughout the year. Pumps are primarily capable of holding liquids, and the transfer of heat dissipation from one heat exchanger to another may vary depending on the unsustainable aspect of the design phase. To streamline the energy and exergy analyses, it was assumed that no loss occurred in the mixer.

The heat input rate from the thermal oil in the evaporator to fluid 1 is calculated as:

$$\begin{aligned} Q_{in} &= m_{wf1}\,(h_1 - h_4) = m_H(h_{H\ In} - h_{H\ Out}) \\ &= m_H * cp_{avg\ oil}\,(T_{H\ In} - T_{H\ Out}) \end{aligned} \tag{1}$$

The rate of work generation in turbines 1 and 2 can be expressed as:

$$W_{t1} = m_{wf1}\,(h_1 - h_{2s})\eta_{p1} = m_{wf1}\,(h_1 - h_2) \tag{2}$$

$$W_{t2} = m_{wf2}\,(h_5 - h_{6s})\eta_{p1} = m_{wf2}\,(h_5 - h_6) \tag{3}$$

The work input rate of fluids 1 and 2 through pumps 1 and 2 can be given as:

$$W_{p1} = \frac{m_{wf1} * (h_{4s} - h_3)}{\eta_{p1}} = m_{wf1}(h_4 - h_3) \tag{4}$$

$$W_{p2} = \frac{m_{wf2} * (h_{9s} - 8)}{\eta_{p2}} = m_{wf2}(h_9 - h_8) \tag{5}$$

The mass fraction of fluid 1 used to heat water in the WHS is calculated as:

$$x = m_{HW} * cp_{HW} * \frac{T_{HW\ OUT} - T_{HW\ In}}{m_{wf1} * (h_2 - h_{2\ WHS})} \tag{6}$$

where m_{HW} (desired mass flow of hot water) is determined from Table 1, and it depends on the demand for hot water and is the factor of water temperature and the ambient temperature in an individual month; m_{HW} is directly proportional to 'x'. 'x' depends on the demand for hot water and is the factor of water temperature and the ambient temperature throughout an individual month.

For heating water in WHS, fluid 1 mass flow rate is calculated using Equation (7).

$$m_{WHS} = x * m_{wf1} \tag{7}$$

The heat transfer rate to water in the WHS is calculated as:

$$Q_{HW} = m_{WHS}\ (h_2 - h_{2\ WHS}\ ) \tag{8}$$

To operate the RORC, mass flow rate of fluid 1 used via the heat exchanger is analysed as:

$$m_{ORC} = (1 - x)\ m_{wf1} \tag{9}$$

Applying the energy balance to a mixer the specific enthalpy $h_{2\ ORC}$ is governed as:

$$h_{2\ ORC} = \frac{(h_3 - x * h_{2\ WHS}\ )}{1 - x} \tag{10}$$

The fluid 2 mass flow rate in RORC is denoted as:

$$m_{wf2} = \frac{m_{ORC}(h_2 - h_{2\ ORC}\ )}{(h_5 - h_{10}\ )} \tag{11}$$

Heat transfer of the working fluid entering the recuperator from turbine exhaust is analysed as:

$$Q_{recup} = m_{ORC}[(h_6 - h_7) + (h_{10} - h_9)] \tag{12}$$

The working fluid heat rejection rate from the condenser to cooling water is expressed as:

$$\begin{array}{rc} Q_{out} & = m_{wf2}(h_7 - h_8) = m_C(h_{C\ Out} - h_{C\ In}) \\ & = m_C * cp_C * (T_{C\ Out} - T_{C\ In}) \end{array} \tag{13}$$

The total net power output of the system is calculated using equation below:

$$W_{net} = W_{t1} + W_{t2} - W_{p1} - W_{p2} \tag{14}$$

The thermal efficiency of the system can be analysed as:

$$\eta_{th} = \frac{W_{net} + Q_{HW}}{Q_{in}} \tag{15}$$

2.3. Exergy Analysis

In thermodynamics, exergy is the greatest possible theoretical power achieved when the system reaches equilibrium with the surroundings. Exergy analysis of a system is very significant because the irreversibility and useful working potential of the system can be clearly understood, and this cannot be defined by energy analysis alone. Variables including exergy destruction and exergy efficiency rate help make model- and economic-based decisions in a design cycle.

The specific flow exergy in any state of a system is expressed as:

$$e = h - h_0 - T_0(s - s_0) \tag{16}$$

By applying the exergy balance equation to the individual components, the exergy destruction of each component is expressed using equations below:

Evaporator:

$$I_{evap} = m_{wf1} * T_0(s_1 - s_4 - (h_1 - h_4)/T_{H\ avg}) \tag{17}$$

Turbines:

$$I_{turbine\ 1} = m_{wf1} * T_0(s_2 - s_1) \tag{18}$$

$$I_{turbine\ 2} = m_{wf2} * T_0(s_6 - s_5) \tag{19}$$

Heat Exchanger:

$$I_{heatexchanger} = m_{ORC\ 1}(e_2 - e_{2\ ORC}) + m_{wf2}(e_{10} - e_5) \tag{20}$$

Pumps:

$$I_{pump\ 1} = m_{wf1} * T_0(s_4 - s_3) \tag{21}$$

$$I_{pump\ 2} = m_{wf2} * T_0(s_9 - s_8) \tag{22}$$

Recuperator:

$$I_{recup} = m_{ORC}(e_6 + e_9 - e_7 - e_{10}) \tag{23}$$

Condenser:

$$I_{condenser} = m_{wf2} * T_0\left(s_8 - s_7 + (h_7 - h_8)/\ T_{C\ avg}\right) \tag{24}$$

Water Heating system:

$$I_{HW} = m_{WHS} * (e_2 - e_{2\ WHS}) + m_{HW} * (e_{HW\ In} - e_{HW\ Out}) \tag{25}$$

The system total exergy destruction is calculated using Equation (26).

$$I_{Total} = I_{evap} + I_{turbine\ 1} + I_{turbine\ 2} + I_{pump\ 1} + I_{pump\ 2} + I_{heatexchanger} + I_{recup} + I_{condenser} + I_{HW} \tag{26}$$

The exergy input rate of the system can be stimulated by the exergy balance of the entire system and is expressed as Equation (27).

$$E_{in} = W_{net} + I_{Total} + \left(\frac{T_0}{T_{HW\ avg}} - 1\right) * Q_{HW} + \left(\frac{T_0}{T_{C\ avg}} - 1\right) * Q_{out} \tag{27}$$

The exergy efficiency of the system is determined as:

$$\eta_{ex} = \frac{W_{net} + m_{HW} * (e_{HW\ Out} - e_{HW\ In})}{E_{in}} \tag{28}$$

2.4. Classification of Working Fluids

The ORC–WHS consists of two ORCs: the top cycle is the SORC and the bottom cycle is the RORC attached to the WHS. Each simulation requires properties of two different working fluids. The choice of ecological and efficient working fluids plays a major role in the overall performance of the ORC. According to the existing literature, there is no ideal working fluid meeting the standard criteria. Depending on different preconditions such as the heat-source temperature and working pressure of the system the optimal working fluid may be different.

Assuming that the system absorbs heat from biogas or the combustion of biomass, it should be a high-temperature heat source for the ORC. The most preferable working fluids for high-temperature ORCs are alkanes, aromatics, and linear siloxanes. Meta-xylene, ethylbenzene, and decane were some alkanes used by Lai et al. [24] in a high-temperature ORC. Thus, these three working fluids and chlorobenzene were used to analyse the SORC in this study. A working fluid with a low critical temperature was recommended for the bottom cycle. Another study [25] stated that the critical temperature of the working fluid should be nearly equal to the source temperature to achieve greater efficiency. KIM [26] recently presented a preliminary study to develop a new cycle layout, and investigate the effect on the working fluids and performance of combined systems (ORC and vapor compression refrigeration cycle) using standard thermodynamic analysis methods.

Considering the environmental issues and good thermodynamic characteristics, we selected a set of five working fluids for RORC analysis of the proposed system: R245fa,

R601 (Propane), R236fa, R1234ze (Z), and R1336mzz (Z). The properties of the working fluids are listed in Table 2.

Table 2. Working fluids properties [27–29].

Working Fluid	Molar Mass (kg/kmol)	Normal Boiling Point (°C)	Critical Pressure (kPa)/Temperature (°C)	ODP/GWP	Safety Group
Top cycle (SORC)					
M-xylene	106.17	139.1	3530/343.7	0/-	A3
Chlorobenzene	112.56	132.1	4520/359.2	-/-	A3
Ethylbenzene	106.17	136.2	3620/344.0	0/-	A3
Decane	142.28	174.2	2103/344.6	0/-	A3
Bottom cycle (RORC)					
R245fa	134.05	15.0	3651/153.9	0/858	B1
R601 (Pentane)	72.15	36.1	3368/196.6	0/11	A3
R236fa	152.04	−1.5	3200/124.9	0/9810	A1
R1234ze (Z)	114.04	9.7	3530/150.1	0/<1	A2L
R1336mzz (Z)	164.06	33.5	2903/171.3	0/2	A1

2.5. Design and Simulation

First the designed system layout was used to evaluate the thermodynamic properties of the selected working fluids. Two independent variables were used for computing other essential state properties. MATLAB [30] was used to analyse and simulate the RORC attached to the WHS. All the thermodynamic properties of working fluids were calculated by using NIST REFPROP [27]. The built-in mathematical functions and simulation conditions allowed the development of arbitrary programs to achieve results by MATLAB. The function provided by REFPROP was used to establish the link between MATLAB and REFPROP for easy analysis of the properties of working fluids.

The examined system design specifications are outlined in this section. Primarily, 2000 kW of heat was transferred by thermal oil to the cycle and circulated through the evaporator. The inlet temperature of thermal oil at 350 °C was used for prime validation. The temperature was subsequently changed from 300 °C to 350 °C to investigate the influence of source temperature on numerous factors for different months; January and August were chosen for the month of winter and summer, respectively. The system was simulated to determine the performance in both the months. The outlet thermal oil temperature was fixed at 240 °C. Although the primary parameters of the cycle are fixed, a difference in cycle input specification and change in performance factors (power and hot water produced by the system) is caused by the deviation in the seasonal temperature input parameters T_0 and $T_{water\ (months),}$ which change throughout the year.

$$Q_{in} = 2000\ \text{kW};\ T_{H\ In} = 300\ ^\circ\text{C} - 350^\circ\text{C};\ \ T_{H\ Out} = 240\ ^\circ\text{C}$$

From Equation (1), the mass flow rate (m_{wf1}) of fluid 1 in circuit 1 can be derived, where Q_{in} is 2000 kW. Here, h_1 and h_4 are known variables governed by two independent attributes at state points 1 and 4, respectively. Equation (29) determines the mass flow rate of fluid 2 (m_{wf2}) in circuit 2.

$$m_{wf1} = \frac{Q_{in}}{(h_1 - h_4)} \tag{29}$$

Turbine and pump isentropic efficiencies were assumed to be 85% and 65% [31], respectively.

$$\eta_{t1} = 0.85\ ;\ \eta_{t2} = 0.85\ ;\ \ \eta_{p1} = 0.65\ ;\ \eta_{p2} = 0.65$$

The inlet temperature of turbine 1 (T_1) was fixed at 30 °C, less than the thermal oil inlet temperature as shown in Equation (30).

$$T_1 = T_{H\ In} - 30 \tag{30}$$

The pressures at states 1 (P_1) and 4 (P_4) were considered to be the saturation pressure at state 1 as indicated in Equation (31)

$$P_1 = P_4 = P_{sat}@T_1 \tag{31}$$

The WHS outlet temperature was set at 35 °C.

$$T_{HW\ Out} = 35°C$$

State 3 (T_3) at the mixer outlet and the 2*WHS* and 2*ORC* outlet states were fixed at 100 °C as indicated in Equation (32), as shown in Figure 1.

$$T_3 = T_{2WHS} = T_{2ORC} = 100°C \tag{32}$$

The inlet temperature of turbine 2 was determined by using Equations (33) and (34).

$$T_5 = T_{5sat} + 5 \tag{33}$$

$$T_{5sat} = T_3 - 10 \tag{34}$$

The pressure at state 3 (P_3) and state 5 (P_5) were indicated by Equations (35) and (36).

$$P_3 = P_{sat}@T_3 \tag{35}$$

$$P_5 = P_{sat}@T_{5sat} \tag{36}$$

where T_{5sat} is the saturation temperature of Working Fluid 2 in the two-phase zone. Superheating of 5 °C occurred before working fluid 2 entered the turbine.

The condensation temperature of RORC was calculated using Equation (37).

$$T_8 = T_{C\ In} + 10 \tag{37}$$

where $T_{C\ In}$ is the inlet temperature of the cooling water entering the RORC condenser.

The RORC condensation pressure was specified using Equation (38).

$$P_8 = P_{sat}@T_8 \tag{38}$$

Monthly ambient temperature was used as the input variable for the system. Likewise, the temperature of the water entering the WHS and RORC condenser was equal to the water temperature accessible every month. Monthly water temperatures are listed in Table 1. The outlet temperature ($T_{C\ Out}$) of the cooling water flow of the RORC condenser is given by Equations (39) and (40).

$$T_{HW\ In} = T_{C\ In} = T_{water\ (month)} \tag{39}$$

$$T_{C\ Out} = T_{C\ In} + 7 \tag{40}$$

3. Results and Discussion

This study examines the periodic (monthly) performance of a RORC–WHS based on energy and exergy analyses. The system operated using heat from a thermal oil circuit. The entire system used two different working fluids. Fluid 2 was used in the bottom RORC, and fluid 1 with a higher critical temperature was used in the SORC. The performance of different parameters, such as net shaft power, power for water heating, thermal efficiency, exergy efficiency, and exergy destruction of individual components was evaluated. Moreover, the temperature of the heat source varied between 300 °C and 350 °C, and the variations in the results of the system thermal efficiencies and exergy destruction for both winter and summer were examined.

To examine the optimal working fluid for the RORC, chlorobenzene was chosen as fluid 1, and a set of five different working fluids [R245fa, R601, R236fa, R1234ze (Z), and R1336mzz (Z)] with low critical temperatures was examined for fluid 2.

Initially, a set of four different working fluids (m-xylene, chlorobenzene, ethylbenzene, and decane) with a high critical temperature was examined for fluid 1 for the SORC. Fluid 2 (R601) was kept constant in the RORC during the analysis. The results are shown in Figure 3a based on exergy efficiency indicate that chlorobenzene exhibits the highest exergy efficiency while decane has the lowest exergy efficiency among the four working fluids.

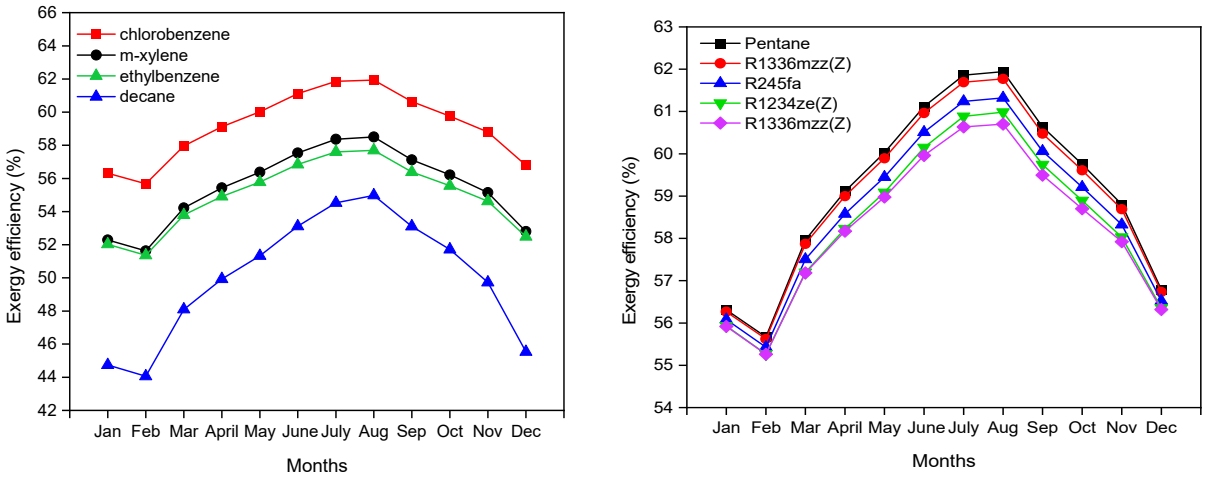

Figure 3. Exergy efficiencies for different months. (**a**) SORC; (**b**) RORC.

To analyse the optimal working fluid for the RORC, chlorobenzene was set as fluid 1, and a set of five different working fluids [R245fa, R601, R236fa, R1234ze (Z), and R1336mzz (Z)] was examined for fluid 2. The exergy curves are shown in Figure 3. As shown in Figure 3b, R601 exhibited the most favourable results. Fluid 1 influenced the exergy efficiency of the cycle more than fluid 2. However, the substitution of fluid 2 by any of the examined working fluids had a minimum effect on exergy as shown in the graph in Figure 3a,b. Exergy efficiency ranged from a minimum of 55.6% to 61.9% in August while winter had a relatively low efficiency. Hence, chlorobenzene was selected as fluid 1 and R601 as fluid 2 in this study.

To analyse the total net shaft power, the same set of four working fluids in the SORC was studied keeping fluid 2 constant as R601 in all cases. Chlorobenzene shows promising results based on the net shaft power as shown in Figure 4a and was selected as fluid 1. Figure 4b indicated R601 as efficient fluid 2 based on the total net shaft curves.

The total shaft power generated via turbines ranged from a minimum of 497.7 kW in January to 585.7 kW in August. Less power was generated in winter than in summer. In winter, the WHS requires more water to heat; therefore, it requires more energy. Energy from the turbine was used to heat water in the WHS supplied via fluid 1. The mass fraction of fluid 1 'x' heated the water, and the fraction '1-x' powered the RORC operation. Changes throughout the year and the change in the generated total shaft power were analysed. It was observed that power generation remained constant via turbine 1, whereas power generated by turbine 2 fluctuated throughout the year.

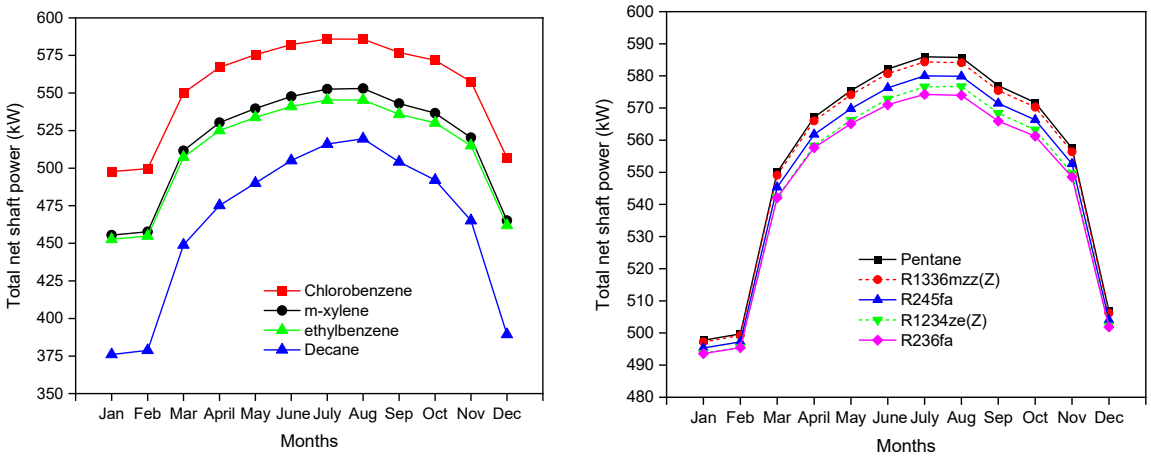

Figure 4. Total net shaft power for different working fluids. (**a**) SORC; (**b**) RORC.

The exergy destruction throughout the year for different components is shown in Figure 5. The exergy destruction value of the WHS fluctuated the most during the year with a maximum value of approximately 244 kW in January and a minimum value of 43.69 kW in August. The requirement for hot water was higher while the ambient temperature was lower during winter, and the demand for hot water was lower while the ambient temperature was higher during summer. Mass fraction x of fluid 1 had a higher rate in winter than in summer while heating water in the WHS. In addition, heat exchangers exhibit higher exergy destruction in summer than that in winter because mass fraction x of fluid 1 heated fluid 2 in the heat exchanger, which was fixed at a higher value in summer. The exergy destruction of pump 1 and the recuperator remained fairly stable throughout the year. Pump 2 showed a greater variation in exergy destruction because the mass flow rate of fluid 2 increased as the heat demand decreased. The rate of destruction in the evaporator and turbine 1 fluctuated slightly during the year with a slight increase in summer (July and August). Compared with turbine 1, the condenser and turbine 2 exhibited greater exergy destruction owing to the change in mass fraction x of fluid 1 that operates RORC.

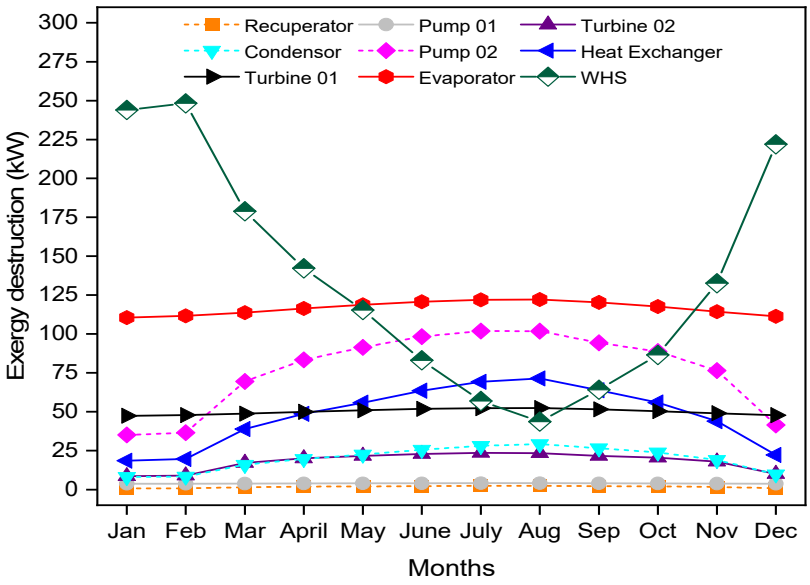

Figure 5. Exergy destruction in individual components of the system.

It can be observed from Figure 3a,b that the system efficiency was lower in winter (November to February) than that in summer (June to September). The primary reason is attributed to the increased demand for hot water and the high amount of exergy destruction of the WHS during winter as shown in Figure 5.

Figure 6 presents the thermal efficiency of SORC and RORC using the selected working fluids. It can be observed that the thermal efficiency in winter was higher than in summer varying from 83.7% in January to 40.3% in August. This is because more heat energy was recovered as more water was heated in the WHS. An increase in m_{WHS} and Q_{HW} values increases the numerator value while the W_{net} state does not substantially decrease. The net impact is the enhancement in the rate of η_{th} throughout winter for a fixed value of Q_{in}.

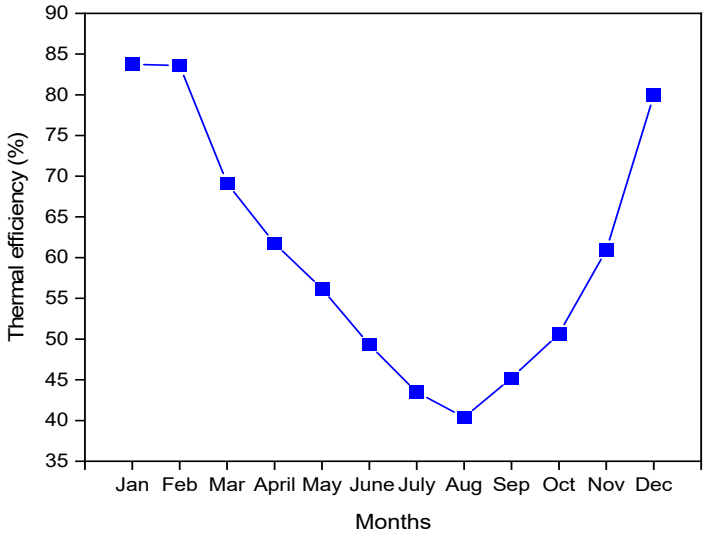

Figure 6. Thermal efficiency of the system using selected working fluids.

The curve in Figure 7 represents the mass fraction x of fluid 1 and the water heating power used for heating water in the WHS. The shapes of both graphs are similar because the power utilised by the WHS is proportional to the mass fraction x of fluid 1 that heats water in the system. The mass fraction 'x' is an input variable based on hot water demand by residents; therefore, it is higher in winter and less in summer. The water heating system consumes more power in winter than in summer.

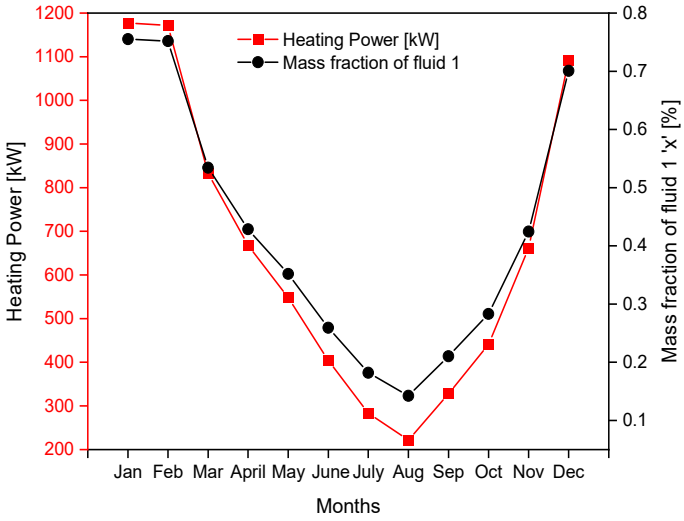

Figure 7. Monthly heating power and mass fraction of fluid 1 'x'.

Another approach was to analyse the system performance in August by changing the heat-source temperature. The variation in the thermal efficiency in August with an increase in the heat source temperature is shown in Figure 8. The turbine inlet temperature increased with increasing heat-source temperature; the system thermal efficiency also increased. A high inlet turbine temperature is proportional to high pressure yielding more work output and resulting in increased thermal efficiency.

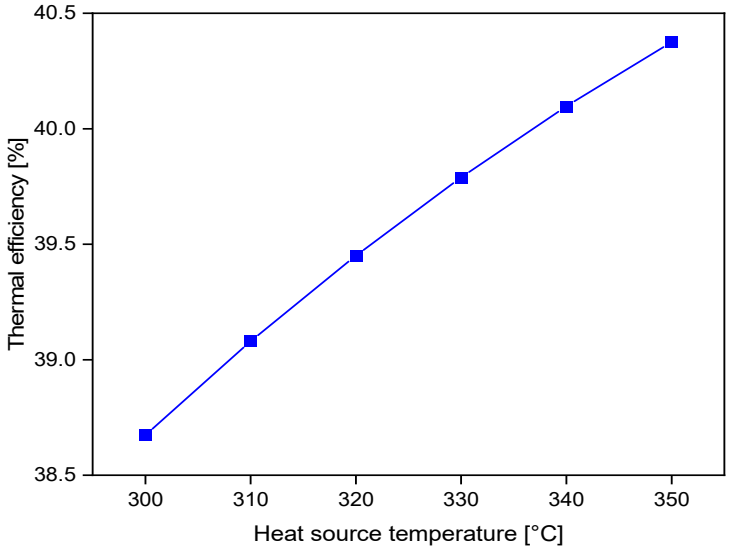

Figure 8. Variation of thermal efficiency with heat source temperature in August.

Figure 9 compares the exergy destruction of different components according to the different heat source temperatures in August. The exergy destruction in the heat exchanger increased with the heat-source temperature. Conversely, the exergy destruction of the WHS did not increase significantly with an increase in the heat-source temperature. The other components exhibited fairly stable exergy destruction. The results in Figure 9 indicate an increase in the total exergy destruction of the system with increasing temperature.

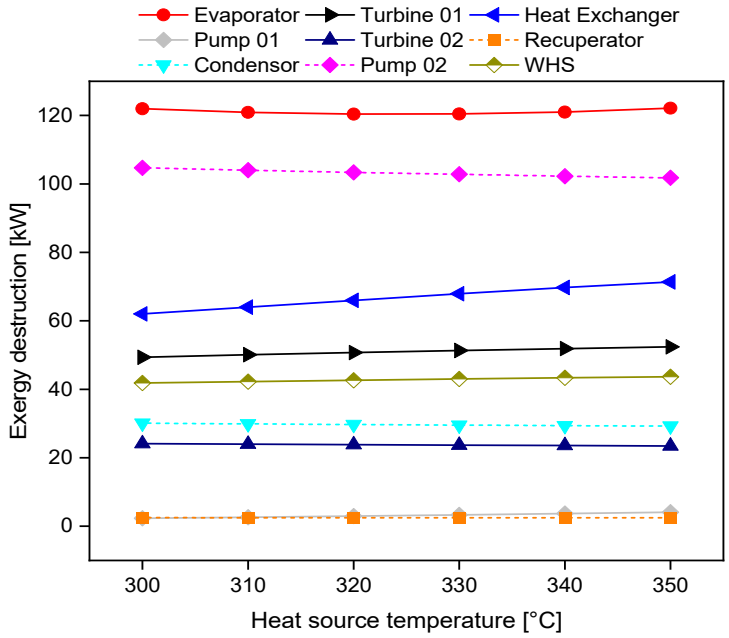

Figure 9. Exergy destruction of different components with different heat source temperatures in August.

The percentage of exergy destruction in the different components of the system at a heat source temperature of 350 °C in August is shown in Figure 10. By comparing the percentage of exergy destruction it can be noted that the evaporator has a maximum of 27% exergy destruction whereas the recuperator has the lowest value of 0.5%.

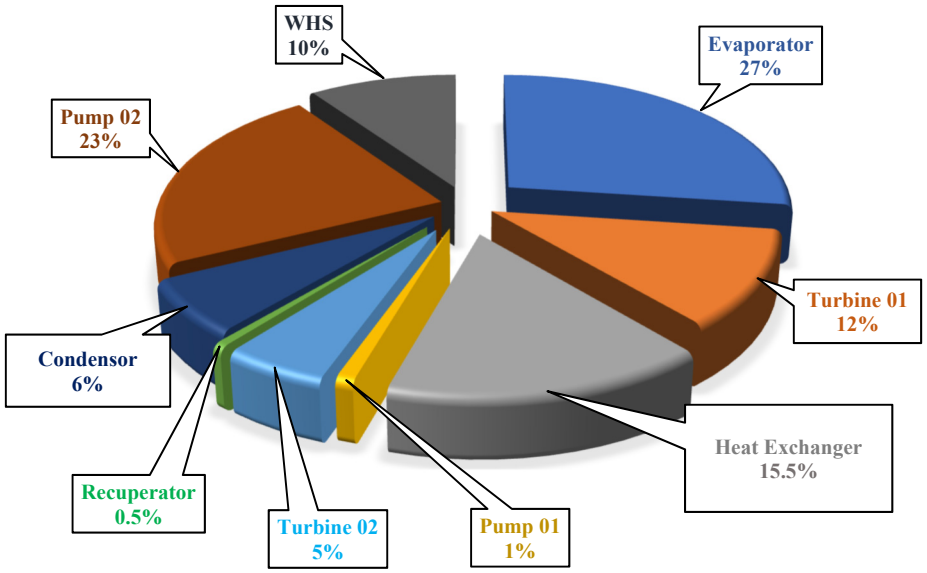

Figure 10. Percentage of exergy destruction in individual components at 350 °C heat source temperature in August.

With an increase in the heat source temperature, there was a small change in the exergy efficiency in increasing order as illustrated in Figure 11. This is because the total net shaft power (Wnet) increases on increasing the heat-source temperature leading to an increase in exergy efficiency. Thus, exergy efficiency is gained by increasing Wnet. Additionally, Wnet is balanced by the exergy efficiency loss due to an increase in the total exergy destruction with a rise in the heat source temperature.

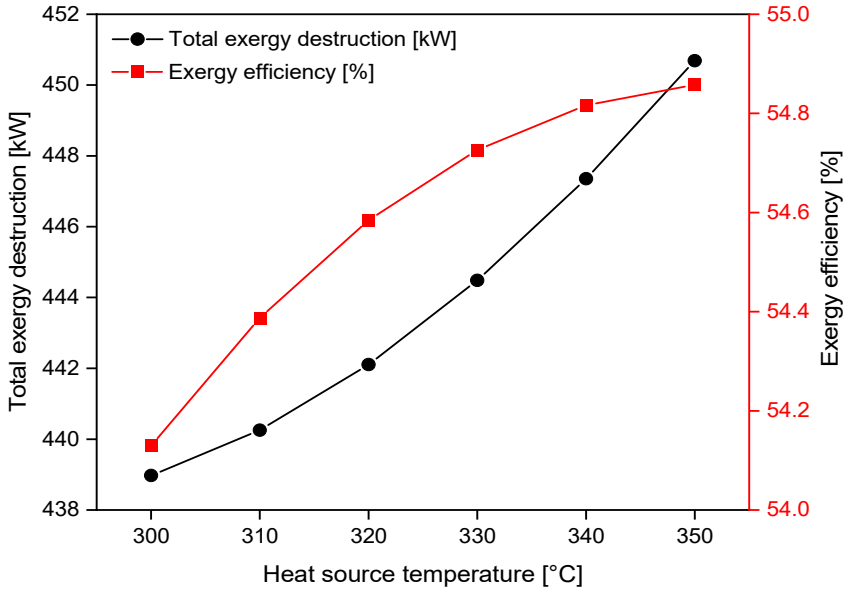

Figure 11. Variation of exergy efficiency and total exergy destruction with heat source temperature in August.

Few differences in the performance of the system were observed in January. Figure 12 illustrates that an increase in the heat source temperature simultaneously increases the thermal efficiency of the system due to the reasons mentioned before. The turbine inlet temperature increases with the heat source temperature, thereby increasing the thermal efficiency of the system.

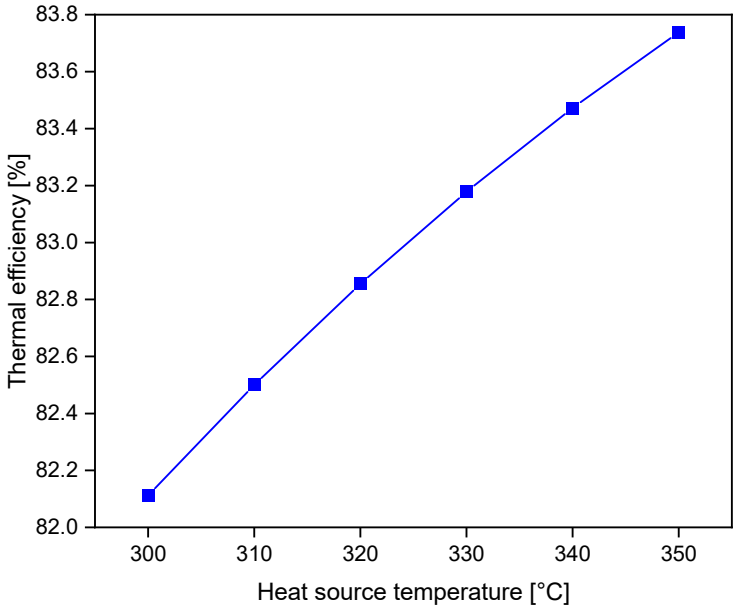

Figure 12. Variation of thermal efficiency with heat source temperature in January.

Destruction of different components due to the different heat source temperatures for January is compared below. In addition to the heat exchanger, the exergy destruction of the WHS also increased with an increase in the heat-source temperature as shown in Figure 13. The exergy destruction value of the WHS in January was higher than that in August because the ambient temperature in January was much lower than that in August. A higher mass flow rate of water had to be heated in January. However, exergy destruction for other components of the system remained relatively constant.

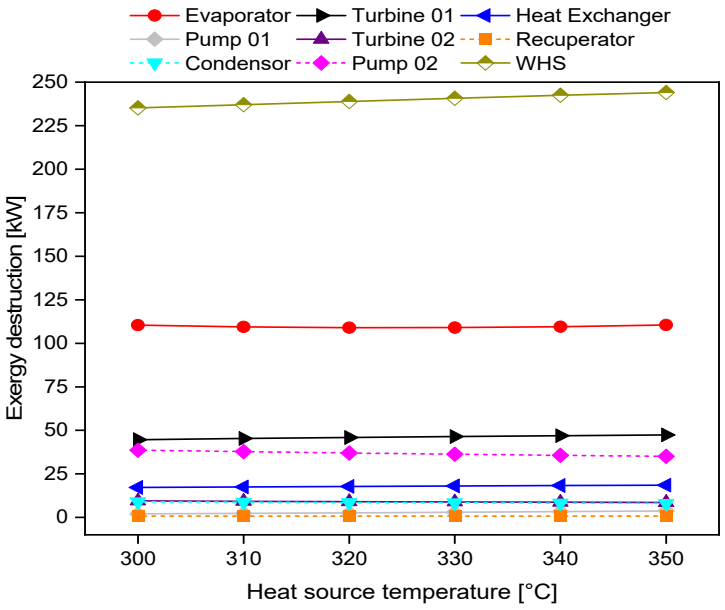

Figure 13. Variation of individual components exergy destruction with heat source temperature in January.

Exergy destruction percentage rates for different components of the system at a heat source temperature of 350 °C in January are shown in Figure 14. The maximum exergy destruction was in the WHS (50.8%), while the recuperator had the smallest exergy destruction (0.2%). Figure 15 shows an increase in the total exergy destruction with an increase in the heat source temperature and similar characteristics for exergy efficiency with increasing heat-source temperature.

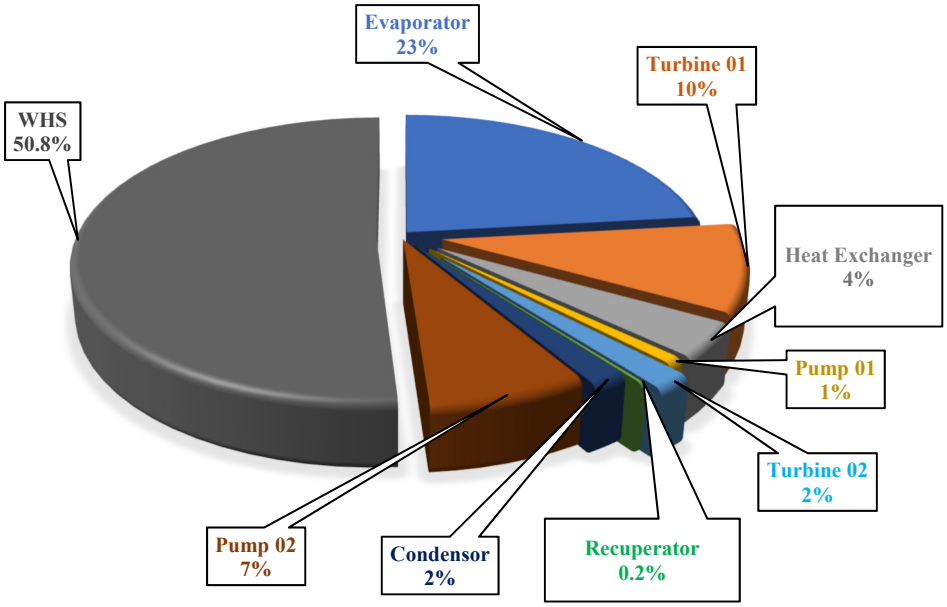

Figure 14. Percentage of individual components exergy destruction at 350 °C heat source temperature in January.

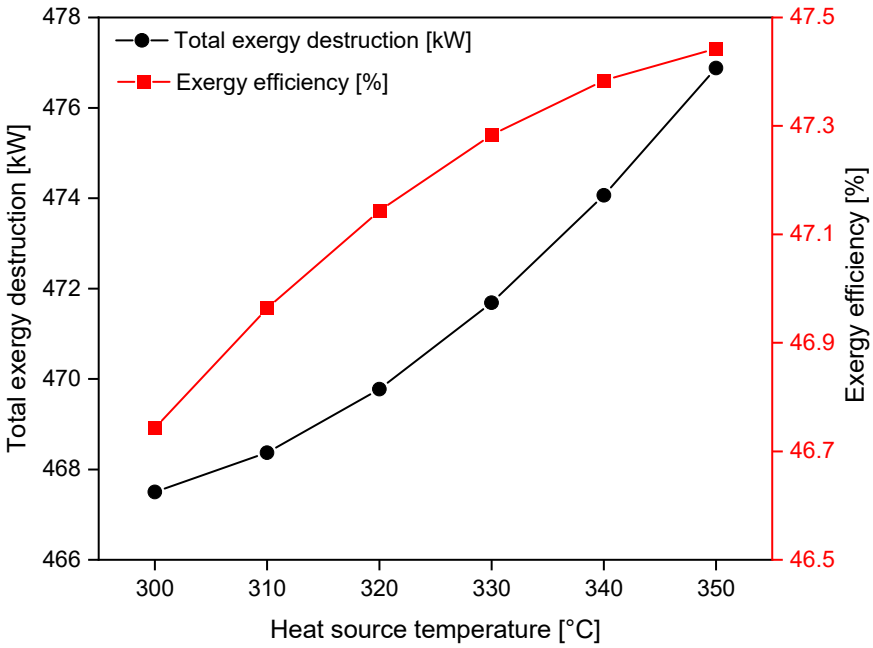

Figure 15. Variation of exergy efficiency and total exergy destruction with heat source temperature in January.

4. Conclusions

The present study investigated the seasonal performance of a recuperative ORC system combined with WHS. The recuperator preserved the excess waste heat to produce a stable

and steady performance of the overall system; the WHS provided hot water to the residents. A wide range of thermodynamic analyses concerning different heat source temperatures were performed, and detailed exergy and energy analyses were conducted in the summer and winter months. The study analysed a set of four and five different working fluids for SORC and RORC systems, respectively.

- A detailed exergy and energy analysis showed the best performance of chlorobenzene in the SORC system during August with maximum exergy efficiency of 61.94% at a fixed heat source temperature of 350 °C and R601 as fluid 2. Although fluid 1 had a significant impact on the cycle efficiency, the optimum performance was obtained with R601 as fluid 2.
- The exergy destruction indicated the WHS, evaporator, and heat exchanger as the main destruction sources. Owing to seasonal changes, the water heating system changed vastly throughout the year depending on the hot water demand. The exergy efficiency during summer was higher than that during winter.
- Thermal efficiency was higher in winter because the water heating system used more energy to heat water and energy utilisation was better.
- The maximum total net shaft power generated by the system was 585.7 kW in August.
- Analysis in January and August showed that an increase in the heat source temperature had a minimum effect on exergy efficiency change but substantially increased the thermal efficiency.

5. Future Work

Additional work can be carried out in the future to analyse and fully utilise the system introduced in this study. The following points describe future work to improve the thermodynamic performance of the system.

- The combined heat and power system (recuperative ORC with water heating system) can be equipped with a refrigeration system to analyse the seasonal performance.
- System optimisation and experimental works will be performed to apply in real industry and society.
- Multi objective optimisation is necessary to improve the thermal economic performance of the system through designing cost and efficiency correlations.

Author Contributions: Conceptualisation, methodology, formal analysis, and original draft preparation by B.K. and M.-H.K. supervised the research and edited the manuscript. All authors have read and agreed to the published version of the manuscript.

Funding: This study received no external funding.

Data Availability Statement: Data is contained within the article.

Conflicts of Interest: The authors declare no conflict of interest.

Abbreviations

CHP	combined heat and power
cp	specific heat capacity [J/kg·K]
E	exergy rate [W]
e	specific exergy of flow [J/kg]
h	Specific enthalpy [J/kg]
I	exergy destruction [W]
m	mass flow rate [kg/s]
η	efficiency
ORC	organic Rankine cycle

Q	heat flowrate[W]
RORC	recuperated ORC
s	specific entropy [J/kg·K]
SORC	simple ORC
T	temperature [K]
W	Power [W]
x	fraction of fluid 1 used to heat water in water heating system
Subscripts	
avg	average
C	cooling water in the condenser
$evap$	evaporator
ex	exergy
H	thermal oil
HW	heating water
In/in	inflow/into the system
0	dead state
Out	outflow/out of the system
$p1,\ p2$	pump 1, pump 2
$recup$	recuperator
s	isentropic
sat	saturation state
$t1,\ t2$	turbine 1, turbine 2
th	thermal
$wf1,\ wf2$	working fluid used in SORC and RORC
WHS	water heating system

References

1. Kim, M.-H.; Pettersen, J.; Bullard, C.W. Fundamental process and system design issues in CO_2 vapor compression systems. *Prog. Energy Combust. Sci.* **2004**, *30*, 119–174. [CrossRef]
2. Kim, M.-H.; Lee, S.Y.; Mehendale, S.S.; Webb, R.L. Microchannel heat exchanger design for evaporator and condenser applications. In *Advances in Heat Transfer*; Academic Press: Cambridge, MA, USA, 2003; pp. 297–429.
3. Khatoon, S.; Almefreji, N.M.A.; Kim, M.-H. Thermodynamic study of a combined power and refrigeration system for low-grade heat energy source. *Energies* **2020**, *14*, 410. [CrossRef]
4. Almefreji, N.M.A.; Khan, B.; Kim, M.-H. Thermodynamic performance analysis of solar based organic rankine cycle coupled with thermal storage for a semi-arid climate. *Machines* **2021**, *9*, 88. [CrossRef]
5. International Energy Agency (IEA). *Korea 2020 Energy Policy Review*; International Energy Agency (IEA): Seoul, Korea, 2020.
6. Climate Scorecard, n.d. Available online: https://www.climatescorecard.org/2020/04/south-koreas-most-recent-energy-plan-focuses-on-energy-conversion/ (accessed on 23 October 2021).
7. Lin, Y.P.; Wang, W.H.; Pan, S.Y.; Ho, C.C.; Hou, C.J.; Chiang, P.C. Environmental impacts and benefits of organic Rankine cycle power generation technology and wood pellet fuel exemplified by electric arc furnace steel industry. *Appl. Energy* **2016**, *183*, 369–379. [CrossRef]
8. Santos, M.; André, J.; Costa, E.; Mendes, R.; Ribeiro, J. Design strategy for component and working fluid selection in a domestic micro-CHP ORC boiler. *Appl. Therm. Eng.* **2020**, *169*, 114945. [CrossRef]
9. Pereira, J.S.; Ribeiro, J.B.; Mendes, R.; André, J.C. Analysis of a hybrid (topping/bottoming) ORC based CHP configuration integrating a new evaporator design concept for residential applications. *Appl. Therm. Eng.* **2019**, *160*, 113984. [CrossRef]
10. Chen, H.; Goswami, D.Y.; Stefanakos, E.K. A review of thermodynamic cycles and working fluids for the conversion of low-grade heat. *Renew Sustain. Energy Rev.* **2010**, *14*, 3059–3067. [CrossRef]
11. Acha, S.; Mariaud, A.; Shah, N.; Markides, C.N. Optimal design and operation of distributed low-carbon energy technologies in commercial buildings. *Energy* **2018**, *142*, 578–591. [CrossRef]
12. White, M.T.; Oyewunmi, O.A.; Chatzopoulou, M.A.; Pantaleo, A.M.; Haslam, A.J.; Markides, C.N. Computer-aided working-fluid design, thermodynamic optimisation and thermoeconomic assessment of ORC systems for waste-heat recovery. *Energy* **2018**, *161*, 1181–1198. [CrossRef]
13. Freeman, J.; Hellgardt, K.; Markides, C.N. Working fluid selection and electrical performance optimisation of a domestic solar-ORC combined heat and power system for year-round operation in the UK. *Appl. Energy* **2017**, *186*, 291–303. [CrossRef]
14. Chatzopoulou, M.A.; Markides, C.N. Thermodynamic optimisation of a high-electrical efficiency integrated internal combustion engine—Organic Rankine cycle combined heat and power system. *Appl. Energy* **2018**, *226*, 1229–1251. [CrossRef]
15. Oyewunmi, O.A.; Kirmse, C.J.W.; Pantaleo, A.M.; Markides, C.N. Performance of working-fluid mixtures in ORC-CHP systems for different heat-demand segments and heat-recovery temperature levels. *Energy Convers. Manag.* **2017**, *148*, 1508–1524. [CrossRef]

16. Aziz, F.; Salim, M.S.; Kim, M.-H. Performance analysis of high temperature cascade organic Rankine cycle coupled with water heating system. *Energy* **2019**, *170*, 954–966. [CrossRef]
17. Nelson, C.R. Application of refrigerant working fluids for mobile organic rankine cycles. In Proceedings of the 3rd International Seminar on ORC Power Systems, Brussels, Belgium, 12–14 October 2015.
18. Zhao, M.; Shu, G.; Tian, H.; Yan, F.; Huang, G.; Hu, C. The investigation of the Recuperative Organic Rankine Cycle models for the waste heat recovery on vehicles. *Energy Procedia* **2017**, *129*, 732–739. [CrossRef]
19. Mago, P.J.; Chamra, L.M.; Srinivasan, K.; Somayaji, C. An examination of regenerative organic Rankine cycles using dry fluids. *Appl. Therm. Eng.* **2008**, *28*, 998–1007. [CrossRef]
20. Wang, J.L.; Zhao, L.; Wang, X.D. An experimental study on the recuperative low temperature solar Rankine cycle using R245fa. *Appl. Energy* **2012**, *94*, 34–40. [CrossRef]
21. Jang, Y.; Lee, J. Optimizations of the organic Rankine cycle-based domestic CHP using biomass fuel. *Energy Convers. Manag.* **2018**, *160*, 31–47. [CrossRef]
22. Yağli, H.; Koç, Y.; Koç, A.; Görgülü, A.; Tandiroğlu, A. Parametric optimization and exergetic analysis comparison of subcritical and supercritical organic Rankine cycle (ORC) for biogas fuelled combined heat and power (CHP) engine exhaust gas waste heat. *Energy* **2016**, *111*, 923–932. [CrossRef]
23. Average Weather in Seoul, South Korea, Year Round—Weather Spark. Available online: https://weatherspark.com/y/142033/Average-Weather-in-Seoul-South-Korea-Year-Round (accessed on 12 May 2021).
24. Lai, N.A.; Wendland, M.; Fischer, J. Working fluids for high-temperature organic Rankine cycles. *Energy* **2011**, *36*, 199–211. [CrossRef]
25. Invernizzi, C.; Iora, P.; Silva, P. Bottoming micro-Rankine cycles for micro-gas turbines. *Appl. Therm. Eng.* **2007**, *27*, 100–110. [CrossRef]
26. Kim, M.-H. Energy and Exergy Analysis of Solar Organic Rankine Cycle Coupled with Vapor Compression Refrigeration Cycle. *Energies* **2022**, *15*, 5603. [CrossRef]
27. Lemmon, E.; Mc Linden, M.; Huber, M. *NIST Standard Reference Database 23: Reference Fluid Thermodynamic and Transport Properties Database: REFPROP Version 10*; NIST: Gaithersburg, MD, USA, 2018.
28. *ANSI/ASHRAE Standard 34-2019*; Designation and Safety Classification of Refrigerants. ASHRAE: Atlanta, GA, USA, 2019.
29. IPCC. *5th Assessment Report—AR5 Synthesis Report: Climate Change 2014*; IPCC: Geneva, Switzerland, 2014.
30. MATLAB—Math Works—R2015a (Version 9.2). 2015. Available online: https://ch.mathworks.com/products/matlab/whatsnew.html (accessed on 15 January 2022).
31. Saleh, B.; Koglbauer, G.; Wendland, M.; Fischer, J. Working fluids for low-temperature organic Rankine cycles. *Energy* **2007**, *32*, 1210–1221. [CrossRef]